**Earthquakes and Structures**, *Vol. 17, No. 3 (2019) 317-327*
DOI: https://doi.org/10.12989/eas.2019.17.3.317


# Modeling the cumulative residual deformation of high-speed railway bridge pier subjected to multiple earthquakes

Hongye Gou[1,2,a], Dan Leng[1b], Longcheng Yang[1c] and Hongyu Jia[*1]

[1]*Department of Bridge Engineering, School of Civil Engineering, Southwest Jiaotong University, Chengdu 610031, China*
[2]*Key Laboratory of High-Speed Railway Engineering, Ministry of Education, Southwest Jiaotong University, Chengdu 610031, China*

*(Received June 23, 2018, Revised April 7, 2019, Accepted June 20, 2019)*

**Abstract.** High-speed railway bridge piers in seismically active area may be subjected to multiple earthquakes and then produce cumulative residual deformation. To study the cumulative residual deformation of high-speed railway bridge piers under multiple earthquakes, a nonlinear numerical analytical model with multi-DOF (MDOF) system is presented and validated against two shaking table tests in this paper. Based on the presented model, a simple supported beam bridge pier model of high-speed railway is established and used to investigate the cumulative residual deformation of high-speed railway bridge pier under mainshock-aftershock sequences and swarm type seismic sequences. The results show that the cumulative residual deformation of the bridge pier increases with earthquake number, and the increasing rates are different under different earthquake number. The residual deformation of bridge pier subjected to multiple earthquakes is accumulated and may exceed the limit of code.

**Keywords:** high-speed railway bridge piers; multiple earthquakes; cumulative residual deformation; nonlinear numerical analytical model with multi-DOF

## 1. Introduction

High-speed railway (HSR) has become the new trend of railway development in the world especially in Asian and European countries due to its high speed, comfort, punctuality, safety and less land use (Sun *et al.* 2016). In China, the running mileage of HSR has been up to 25000 kilometers by the end of 2017. With the implementation of national important strategies proposed during the "Thirteenth Five-Year Plan" period, such as "One Belt, One Road", the construction of high-speed railway is gradually transferred to the Midwest of China (Zheng *et al.* 2014). The mileage of HSR is increasing in seismically active area.

As one of the infrastructure of high-speed railway system, bridges account for more than 50% of the total HSR mileage (Yan *et al.* 2015). For some special HSR lines, bridges are even up to 90%. In seismically active area, these high-speed railway bridges may be subjected to multiple earthquakes (Abdelnaby and Elnashai 2015, Rostamian *et al*. 2017, Kostinakis and Morfidis 2017). And then the cumulative residual deformation of pier will be produced. Existing studies have shown that the effect of common cumulative residual deformation of piers on track regularity cannot be ignored, because the track regularity directly affects the running safety and riding comfort of trains (Tutumluer *et al*. 2013, Ju *et al*. 2014, Gou *et al.* 2018). Therefore, it is necessary to investigate the cumulative residual deformation of high-speed railway bridge piers under multiple earthquakes.

In recent decades, the residual deformation and vulnerability assessment of structures under multiple earthquakes have attracted more and more attention from domestic and foreign scholars. Based on the elastic-plastic hysteretic model of stiffness degradation and the shaking table tests of reinforced concrete members, Yazgan and Dazio (2011, 2012) pointed out that the fiber element model can be used to accurately calculate the residual deformation of reinforced concrete members. Thus, many fiber element models based on different material constitutive relation were established to study the residual deformation of reinforced concrete members under multiple earthquakes (Lee and Billington 2010, Saiidi and Ardakani 2012, Guo *et al.* 2016). And some shaking table tests were also used by other researchers to study the residual deformation of structures under multiple earthquakes (Dai *et al.* 2017, Benavent-Climent *et al.* 2018, Zheng *et al.* 2018). Moreover, many ways to calculate the residual deformation and assess the fragility were proposed. Ruiz-Garcia and Miranda (2010) proposed a probability model method for calculating the residual deformation of the multi-story framed building and determined the demand of residual deformation for structures under different requirements for seismic resistance. Zhang *et al.* (2013) presented a simplified method, which was suitable for Kinematic hysteretic model and Takeda hysteretic model, to calculate the residual deformation. Hatzigeorgiou *et al.* (2011) constructed empirical equations for a simple and effective determination of the maximum seismic deformation from

*Corresponding author, Associate Professor
E-mail: Hongyu1016@swjtu.edu.cn
[a]Professor
E-mail: gouhongye@swjtu.cn
[b]Master Student
E-mail: 842006596@qq.com
[c]Master Student
E-mail: 1106461245@qq.com



ISSN: 2092-7614 (Print), 2092-7622 (Online)

residual displacements, which was applied both to far-field and near-field ground motions. Alessandri *et al.* (2013) presented a method for evaluating post-earthquake bridge practicability based on a rational combination of information derived from numerical analyses and in situ inspection. Jalayer and Ebrahimian (2017) proposed a formulation to calculate the limit state exceedance probability of structure due to a sequence of mainshock and the triggered aftershocks. Omranian *et al.* (2018) used a cloud analysis method subjected to a wide range of as-recorded sequences to perform the seismic fragility assessment of RC skew bridge subjected to mainshock and aftershocks. However, the studies mentioned above focused on the residual deformation of structures under single earthquake and mainshock-aftershock sequences. Besides, the research objectives were mainly simplified single DOF system and building frame structure. There is a lack of studies on the cumulative residual deformation of structures under swarm type seismic sequences, especially the high-speed railway bridge piers with MDOF system.

In this paper, a nonlinear numerical analytical model with MDOF system is proposed on the basis of considering flexural deformation of structure and slippage of reinforcement. Then, based on the presented model, the high-speed railway bridge pier model with MDOF system is established. Next, mainshock-aftershock sequences and swarm type seismic sequences are constructed as the input ground motions. Finally, the cumulative residual deformation of high-speed railway bridge pier is investigated by calculating displacement-time curves of pier top under different earthquake sequences.

## 2. Nonlinear numerical analytical model based on nonlinear beam-column element

### *2.1 Residual deformation at nonlinear beam-column element*

The nonlinear beam-column element was proposed by Filippou. To obtain the residual deformation of an element, an element is divided into several integral regions. The section forces $F(x)$ of the integration points, which relates the element forces $Q$, is expressed as

$$F(x) = b(x) \bullet Q \tag{1}$$

$$b(x) = \begin{bmatrix} \frac{x}{L} - 1 & \frac{x}{L} & 0 \\ 0 & 0 & 1 \end{bmatrix} \tag{2}$$

where $x$ is the $x$ coordinate of the integration point in the global coordinate system, and $L$ is the length of the member.

According to the section forces $F(x)$ and section flexibility matrix $f(x)$ of last iterative step, the section deformation $d(x)$ can be obtained

$$d(x) = f(x) \bullet F(x) \tag{3}$$

Using the relationship between the section forces $F(x)$ and the corresponding deformations $d(x)$, the section resisting forces $D_R(x)$ can be obtained

$$D_{\mathrm{R}}(x) = k(x) \bullet d(x) \tag{4}$$

$$k(x) = \begin{bmatrix} \sum_{i=1}^{n} E_i A_i y_i^2 & -\sum_{i=1}^{n} E_i A_i y_i \\ -\sum_{i=1}^{n} E_i A_i y_i & \sum_{i=1}^{n} E_i A_i \end{bmatrix} \tag{5}$$

where $n$ is the total number of fibers in the section, $E_i$ is the initial tangent modulus of the $i$th fiber, $A_i$ is the initial area of the $i$th fiber, and $y_i$ is the $y$ coordinate of the $i$th fiber in the local-coordinate system.

If the section forces $F(x)$ and the section resisting forces $D_R(x)$ are not equal, the unbalanced forces of section will be transformed into the residual deformation of section.

$$r(x) = f(x) \bullet (F(x) - D_{\mathrm{R}}(x)) \tag{6}$$

The element deformation increment of next iterative step can be obtained by integrating along the length.

$$\Delta q^{j+1} = -s^j = \int_0^L b^T(x) r(x) dx \tag{7}$$

where $\Delta q^{j+1}$ is the deformation increment of an element in step $j$+1, and $s^j$ is the residual deformation of an element in step $j$.

The iteration mentioned above will continue until the section forces $F(x)$ and the section resisting forces $D_R(x)$ are equal, namely the unbalanced forces are zero. And the above process is called internal iteration of element, which makes iterative convergence speed of the whole structure greatly improved (Chen *et al.* 2011).

### *2.2 Nonlinear numerical analytical model*

In this study, the nonlinear numerical analytical model with MDOF system consisted of five nonlinear beam-column elements in OpenSees, as shown in Fig. 1. To satisfy the precision and improve the computational efficiency, each element was set up with five integral points. The sections of element were divided into many fibers, including concrete fibers and reinforcing steel fibers. The concrete fibers are in the state of tension and compression alternately under earthquakes, and cracking may occur (Jiang *et al.* 2013). Therefore, the cover concrete fibers are usually simulated by the Concrete01 with simple constitutive model and considering the confinement of stirrup (Abbiati *et al.* 2015, Kurt *et al.* 2011, Pragalath *et al.* 2016); the core concrete fibers are simulated by the Concrete01WithSITC which can well capture the residual deformation of members after earthquakes (Lee and Billington 2007). Except that, the Concrete02 considering the mechanical properties of concrete in tension can be also used to simulate the core concrete fibers (Sun *et al.* 2014), and the Concrete04 considering the stiffness degradation of concrete in elastic and cracking stage can be used to simulate the all concrete fibers (Akpınar and Binici 2013). The reinforcing steel fibers in the pier are simulated by the Steel02 which is proposed on the basis of Giuffre-Menegotto-Pinto model and consider the Bauschinger effect of reinforcing steel (Han *et al.* 2010, Moghaddasi and

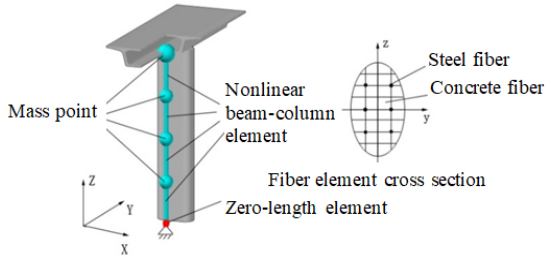


Fig. 1 Nonlinear numerical analytical model based on nonlinear beam-column element

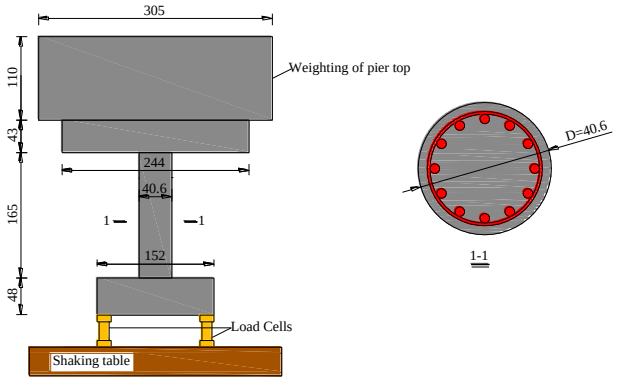


Fig. 2 Geometry of the reinforced concrete single column pier (unit: cm)

Zhang 2013, Shafaei *et al.* 2014). The reinforcing steel fibers at the bottom of the pier, namely on the zero-length element, are simulated by the Bond_SP01 which can take into account the slippage of reinforcing steel (Sun *et al.* 2014). The loads on the pier include its deadweight and the vertical load on the top of the pier. The mass of the pier is equally distributed into each node according to the lumped mass method. The mass converting from the counterweight or load on the top of the pier is added to the node on the top of the pier.

### *2.3 Validation of nonlinear numerical analytical model*

In general, model test and In-situ test have been considered as the effective approaches to investigate the mechanical performance of bridge structures (Gou *et al.* 2018a-e). Thus, Sakai *et al.* (2005) and Choi *et al.* (2010) respectively completed the shaking table test of single column piers under single earthquake and the shaking table test of cantilevered reinforced concrete piers under multiple earthquakes to study the seismic behavior of reinforced concrete piers. In this section, the two reinforced concrete piers mentioned above were modeled and used to verify the presented nonlinear numerical analytical model.

#### *2.3.1 Validation of nonlinear numerical analytical model under single earthquake*

A reinforced concrete single column pier tested by Sakai *et al.* in Berkeley branch School of California University is used to verify the nonlinear numerical analytical model under single earthquake. The geometry of the reinforced concrete single column pier is shown in Fig. 2, and the material properties of longitudinal reinforcing steel and concrete are shown in Table 1 and Table 2, respectively. The vibration table was bidirectional, the axial pressure was applied by the deadweight of the rectangular concrete block on the top of the pier, and the *P*-Δ effect was also considered. The two horizontal components of a modified motion recorded in Los Gatos during the 1989 Loma Prieta, California, earthquake were selected for the test input signals. The waveforms are shown in Fig. 3. To investigate nonlinear dynamic response of the pier, the intensity of the ground motion was set to develop a displacement ductility of about 4 in the earthquake simulator test program (Sakai *et al.* 2005), and the amplitude scaling factor for the ground motion intensity was 0.7. Moreover, free vibration for 10 s was added to obtain the residual deformation.

The test pier is modeled by the nonlinear numerical analytical model with MDOF system. The core concrete

Table 1 Material properties of longitudinal reinforcing steel

| Yield strength (MPa) | Ultimate strength (MPa) | Elastic modulus (MPa) | Hardening rate |
|---|---|---|---|
| 491 | 728 | 210000 | 0.02 |

Table 2 Material properties of concrete

| Material | Peak stress (MPa) | Peak strain | Ultimate stress (MPa) | Ultimate strain | Elastic modulus (GPa) |
|---|---|---|---|---|---|
| Confined concrete | 45.03 | 0.006 | 39.291 | 0.017 | 28.15 |
| Unconfined concrete | 31.7 | 0.002 | 0 | 0.004 | 28.15 |

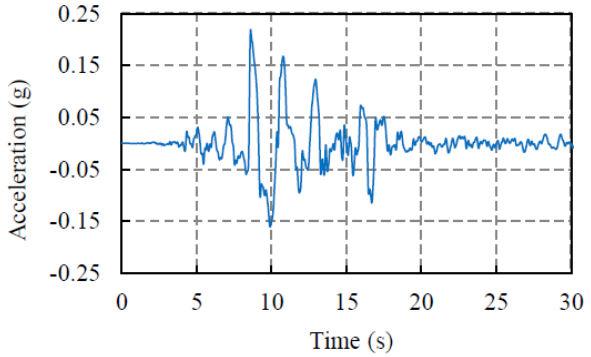


(a) *X* direction

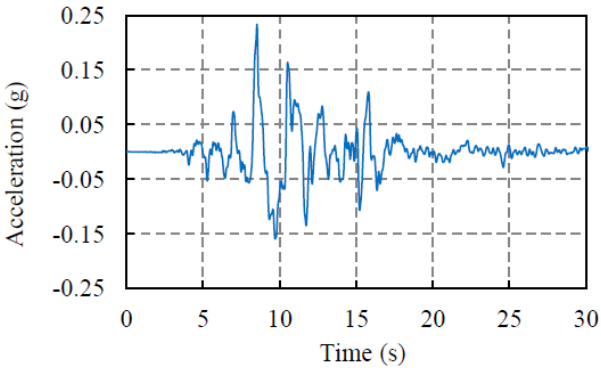


(b) *Y* direction

Fig. 3 Seismic waveforms

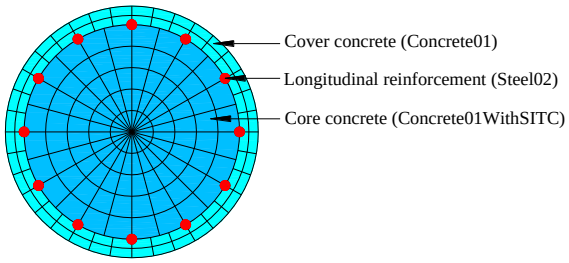


Fig. 4 Fiber section of the reinforced concrete single column pier model

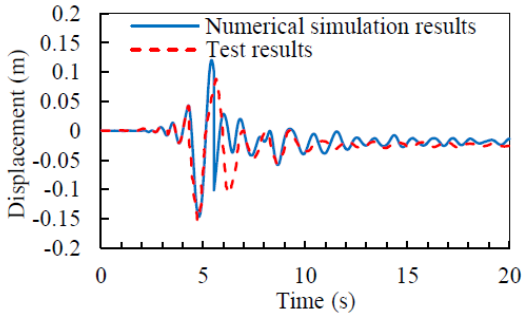


(a) *X* direction

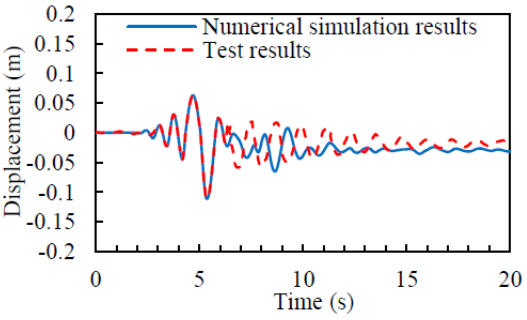


(b) *Y* direction

Fig. 5 Displacements of pier top

Table 3 Maximum and residual distances of pier top

| | Maximum displacement in *X* direction | Maximum displacement in Y direction | Vector sum of residual deformation |
|---|---|---|---|
| Numerical simulation results (mm) | 147 | 111 | 33.15 |
| Test results (mm) | 155 | 105 | 31 |
| Deviation | 4% | 5.7% | 6.9% |

fibers are simulated by the Concrete01WithSITC, the cover concrete fibers are simulated by the Concrete01, the reinforcing steel fibers in the pier are simulated by the Steel02, and the reinforcing steel fibers at the bottom of the pier are simulated by the Bond_SP01. The fiber section of the model is shown in Fig. 4. Under the above ground motion, the displacement and residual deformation of pier top are obtained and compared with test results, as shown in Fig. 5 and Table 3.

It can be seen in Fig. 5 that the displacements of pier top obtained by the nonlinear numerical analytical model and the shaking table test coincide well in the first 5s. Around 5 seconds, the maximum displacement of pier top appears.

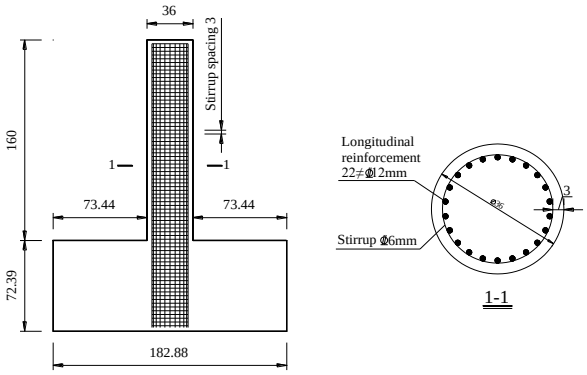


Fig. 6 Geometry of the cantilevered reinforced concrete pier (unit: cm)

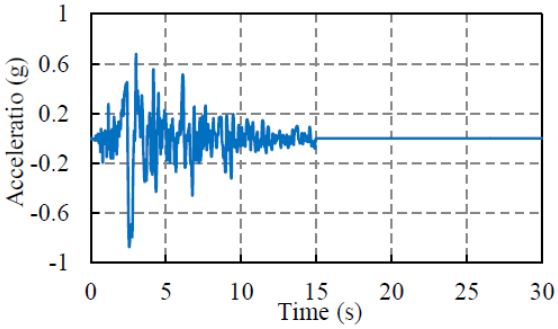


Fig. 7 Seismic waveform

Then there is deviation between the numerical simulation results and the test results, which is caused by the sparse fiber section mesh or fewer elements. In Table 3, it can be seen that the maximum displacement and the residual deformation obtained by the nonlinear numerical analytical model and the shaking table test agree well, and the deviations are not more than 10%. Therefore, the nonlinear numerical analytical model can be used to study the residual deformation of bridge piers under single earthquake.

### *2.3.2 Validation of nonlinear numerical analytical model under multiple earthquakes*

To verify the nonlinear numerical analytical model under multiple earthquakes, a cantilevered reinforced concrete pier tested by Choi *et al.* in the University of Nevada-Reno (UNR) is selected to model. The geometry of the cantilevered reinforced concrete pier is shown in Fig. 6. The reinforcing steel had a yield strength of 490 MPa, and the concrete had a compressive strength of 44.1 MPa. The axial pressure was applied by the prestressed steel strand anchored on the top of the pier and at the bottom of the pier, and the axial compression ratio was 0.08. The ground motion recorded by the Rinaldi Station in the Northridge earthquake in 1994, as shown in Fig. 7, was selected for the test input seismic loads. And free vibration for 15 s was added to obtain the residual deformation. Because of the damage of the pier and the limit of the shaking table, a total of 12 shaking table tests were carried out under ground motions with the same waveforms but different peak ground accelerations (0, 0.04, 0.08, 0.17, 0.25, 0.38, 0.50, 0.63, 0.75, 0.88, 1.01, and 1.13).

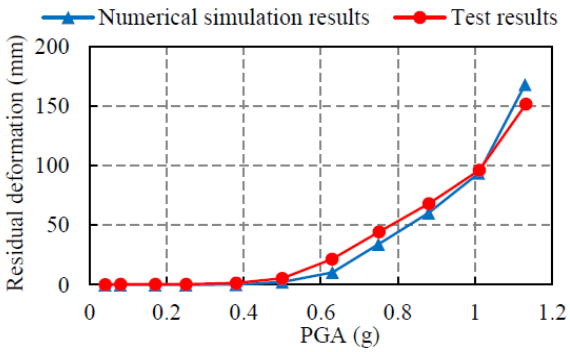


Fig. 8 Residual deformations of pier

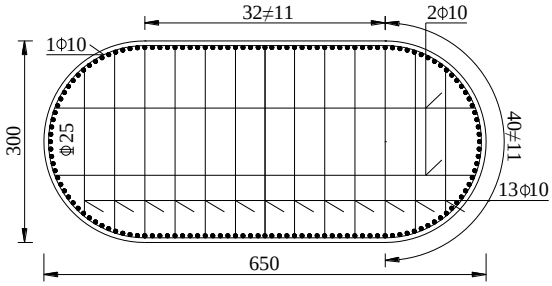


Fig. 9 Cross section and reinforcement of the high-speed railway simple supported beam bridge pier (unit: cm)

The test pier is modeled by the nonlinear numerical analytical model with MDOF system. The cover concrete fibers are simulated by the Concrete01, the core concrete fibers are simulated by the Concrete02, the reinforcing steel fibers in the pier are simulated by the Steel02, and the reinforcing steel fibers at the bottom of the pier are simulated by the Bond_SP01. Under the above ground motion, the residual deformations of pier are obtained and compared with test results, as shown in Fig. 8. The simulation and test results coincide well. Therefore, the nonlinear numerical analytical model can be used to study the residual deformation of bridge piers under multiple earthquakes.

## 3. Modeling of the high-speed railway bridge pier

Compared with highway bridge piers, the aspect ratio of the high-speed railway bridge pier is larger, but the longitudinal reinforcement ratio is lower. To ensure the running safety and riding comfort of trains, the longitudinal and transverse stiffness of the high-speed railway bridge pier are also greater than that of normal railway bridge pier. At present, the high-speed railway bridge pier forms mainly include solid pier with round ended cross-section, hollow pier with round ended cross-section, solid pier with rectangular cross-section, hollow pier with rectangular cross-section, single cylindrical pier, and double cylindrical pier in China. In this paper, a solid pier with round ended cross-section is selected to investigate the cumulative residual deformation of the high-speed railway bridge pier.

### *3.1 The high-speed railway bridge pier structure*

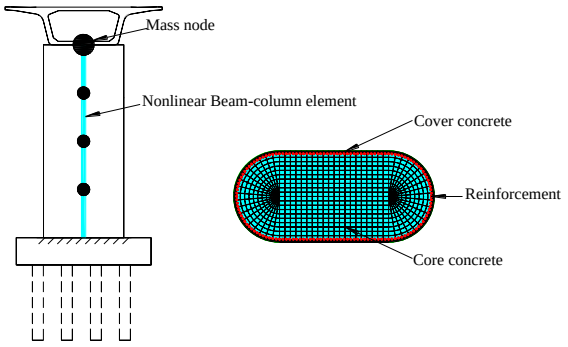


Fig. 10 High-speed railway simple supported beam bridge pier model

The high-speed railway bridge pier investigated in this paper is in the Beijing-Shenyang Railway Line. The height of the pier is 32 m. The length of cross section is 650 cm, and the breadth of cross section is 300 cm, as shown in Fig. 9. The concrete is C35, the longitudinal reinforcing bars are HRB400 with diameter of 25 mm, and the stirrups are HPB300 with diameter of 10 mm.

### *3.2 The high-speed railway bridge pier model*

The high-speed railway bridge pier model with MDOF system is shown in Fig. 10. Since the pile-soil interaction is not considered, the pier model only consists of four nonlinear beam-column elements, and the zero-length element was not established. The concrete fibers are simulated by the Concrete04, the reinforcing steel fibers are simulated by the Steel02. The mass of the pier is equally distributed into each node. The mass of bridge girder is added to the node on the top of the pier.

## 4. The input earthquake sequences

In general, there are three types of earthquake sequence, including mainshock-aftershock sequence, swarm type seismic sequence and isolated type seismic sequence. According to literatures (Wu *et al.* 1990, Zhou *et al.* 1980), the mainshock-aftershock sequence accounts for 60%, the swarm type seismic sequence accounts for 25%, and the isolated type seismic sequence accounts for 15%. Therefore, three mainshock-aftershock sequences and two swarm type seismic sequences are constructed as the input ground motions to study the cumulative residual deformation of the high-speed railway bridge pier subjected to multiple earthquakes.

### *4.1 Three mainshock-aftershock sequences*

The mainshock-aftershock sequences are constructed by the ground motions selected from the Pacific Earthquake Engineering Research Center (PEER) database, as shown in Table 4. All ground motions are intercepted and baseline corrected to remove the seismic waves that had no significant effect on the structure and avoid the “drift” of velocity or displacement. The peak ground acceleration

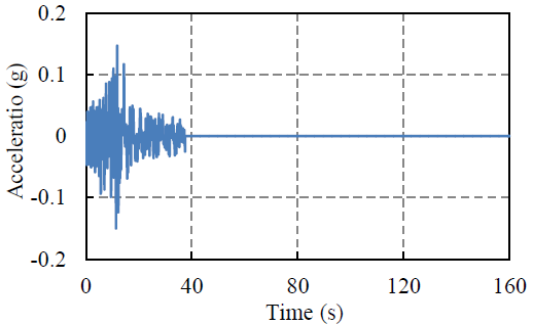


(a) *X* direction

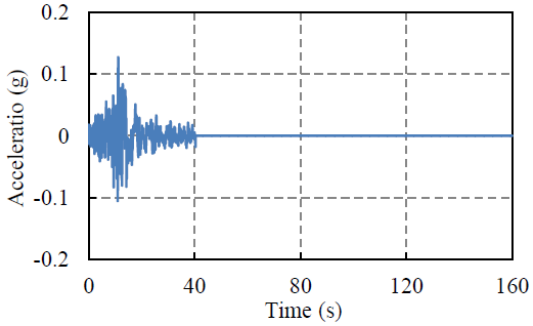


(b) *Y* direction

Fig. 11 CHICHI_CHY101_1244 Seismic waveforms

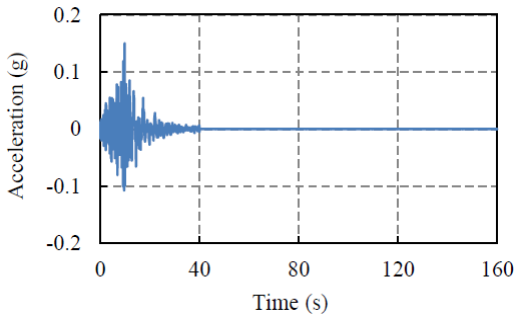


(a) X direction

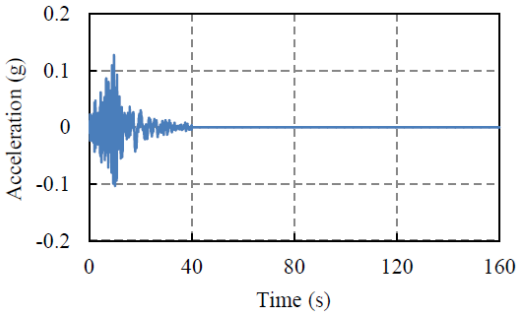


(b) Y direction

Fig. 12 CHICHI_CHY101_2752 seismic waveforms

Table 4 Mainshock-aftershock sequences

| Earthquake sequence number | Record number | Station | Name | Type | Peak ground acceleration (g) |
|---|---|---|---|---|---|
| 1 | 1503 | TCU065 | Chi-Chi, Taiwan | Main shock | 0.150 |
| | 2382 | TCU065 | Chi-Chi, Taiwan-02 | Aftershock | 0.117 |
| | 2618 | TCU065 | Chi-Chi, Taiwan-03 | Aftershock | 0.117 |
| | 3467 | TCU065 | Chi-Chi, Taiwan-06 | Aftershock | 0.117 |
| 2 | 1244 | CHY101 | Chi-Chi, Taiwan | Main shock | 0.150 |
| | 2507 | CHY101 | Chi-Chi, Taiwan-03 | Aftershock | 0.117 |
| | 2752 | CHY101 | Chi-Chi, Taiwan-04 | Aftershock | 0.117 |
| | 3317 | CHY101 | Chi-Chi, Taiwan-06 | Aftershock | 0.117 |
| 3 | 1100 | Abeno | Kobe_ Japan | Main shock | 0.150 |
| | 1104 | Fukushima | Kobe_ Japan | Aftershock | 0.109 |
| | 1110 | Morigawachi | Kobe_ Japan | Aftershock | 0.109 |
| | 1118 | Tadoka | Kobe_ Japan | Aftershock | 0.109 |
| | 1121 | Yae | Kobe_ Japan | Aftershock | 0.109 |

(PGA) of the main shock is adjusted to 0.15 g, and the PGAs of the aftershocks are determined according to the method proposed by Hatzigeorgiou and Beskos (2009). The ratio of PGAs in *X* direction and *Y* direction is 1:0.85 (GB 50011-2010, Code for Seismic Design of Buildings). In addition, zero acceleration for 3t (t was the duration of last ground motion) was added between each seismic wave to obtain the residual deformation.

### *4.2 Two swarm type seismic sequences*

The swarm type seismic sequences are constructed by the two seismic waves recorded by the CHY101 Station in the 1999 Chi-Chi Earthquake, as shown in Fig. 11 and Fig. 12. The two seismic waves are numbered 1244 and 2752, respectively. The intensity and duration of each earthquake are assumed to be the same, and the seismic waves are repeated. In addition, there is a time interval of 3t (t was the duration of last ground motion) between each seismic wave to obtain the residual deformation.

## 5. Results and discussion

### *5.1 Cumulative residual deformation under mainshock-aftershock sequences*

The displacements of pier top in *X* direction and *Y* direction under mainshock-aftershock sequences are displayed in Fig. 13, Fig. 14 and Fig. 15, respectively. It can be seen that the maximum displacement of the pier and the residual deformation of the pier are different under mainshock-aftershock sequences. Thus, there is no direct relationship between the maximum displacement and the residual deformation of the pier under mainshock-aftershock sequences. Besides, the maximum displacement of the pier under aftershocks is much smaller than that under main shock in Fig. 13(a). The reason is that the acceleration of aftershocks in the mainshock-aftershock sequence 1 is less than 0.05 g in most time, even the PGA

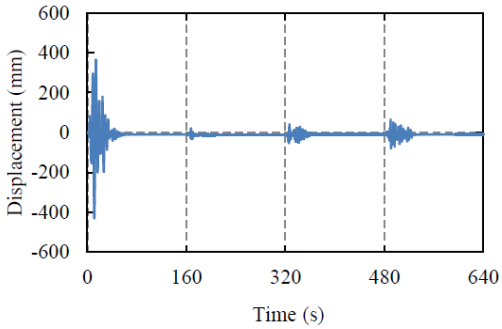


(a) *X* direction

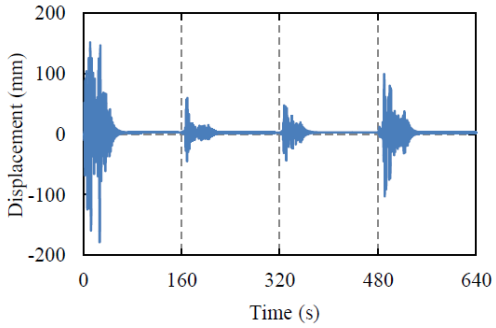


(b) *Y* direction

Fig. 13 Displacements of pier top under the mainshock-aftershock sequence 1

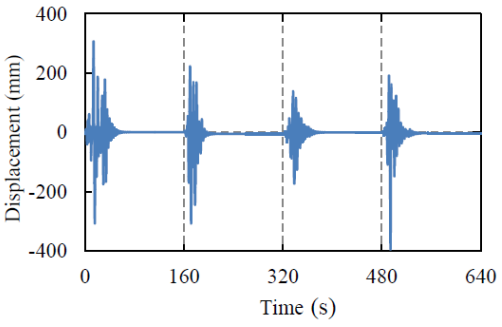


(a) *X* direction

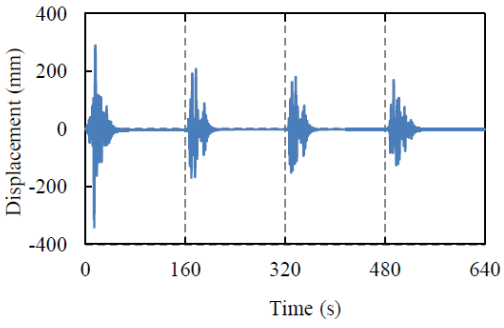


(b) *Y* direction

Fig. 14 Displacements of pier top under the mainshock-aftershock sequence 2

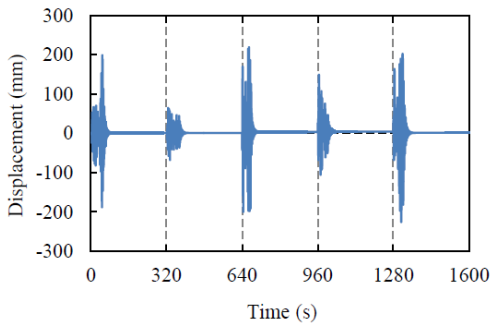


(a) *X* direction

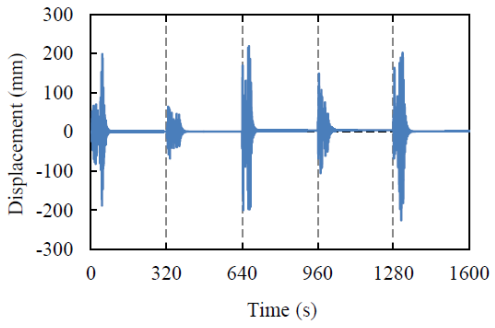


(b) *Y* direction

Fig. 15 Displacements of pier top under the mainshock-aftershock sequence 3

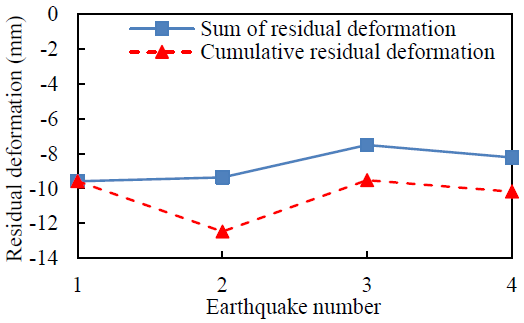


(a) *X* direction

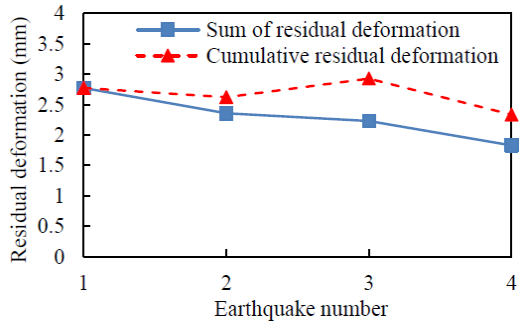


(b) *Y* direction

Fig. 16 Cumulative residual deformations under the mainshock-aftershock sequence 1 and sums of residual deformation under mainshock and aftershocks of the mainshock-aftershock sequence 1

of aftershocks is 0.117 g. Therefore, the factors influencing maximum displacement of pier under mainshock-aftershock sequences are not only the PGA, but also the duration of acceleration.

To study the influence of damage in the last earthquake on residual deformation in the next earthquake, the cumulative residual deformations of the pier under mainshock-aftershock sequences and the sums of residual deformation of the pier under mainshocks and aftershocks are compared, as shown in Fig. 16, Fig. 17 and Fig. 18. The

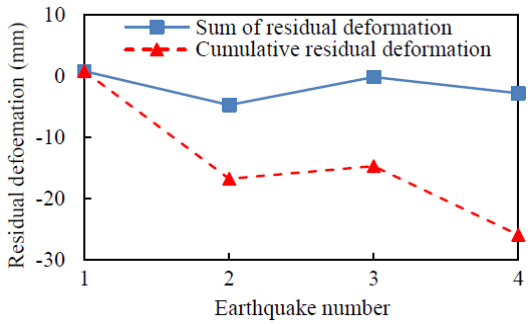


(a) X direction

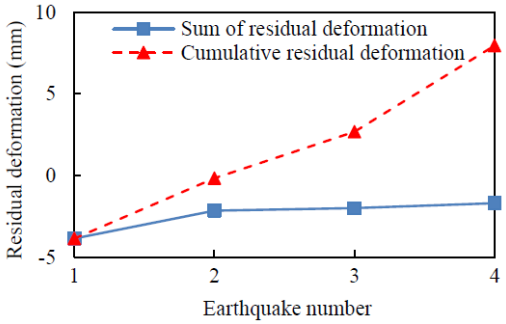


(b) Y direction

Fig. 17 Cumulative residual deformations under the mainshock-aftershock sequence 2 and sums of residual deformation under mainshock and aftershocks of the mainshock-aftershock sequence 2

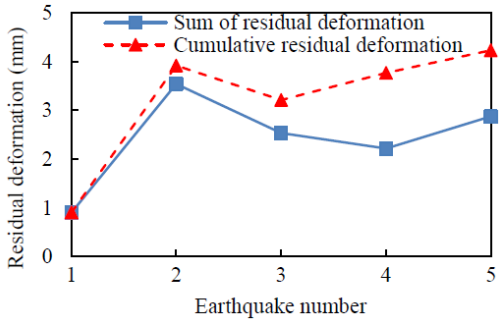


(a) *X* direction

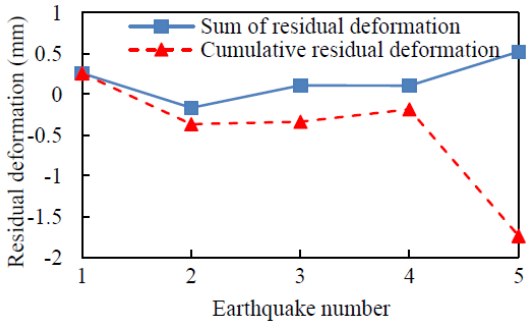


(b) *Y* direction

Fig. 18 Cumulative residual deformations under the mainshock-aftershock sequence 3 and sums of residual deformation under mainshock and aftershocks of the mainshock-aftershock sequence 3

cumulative residual deformation of the pier considers the damage of the pier in the last earthquake sequence, but the

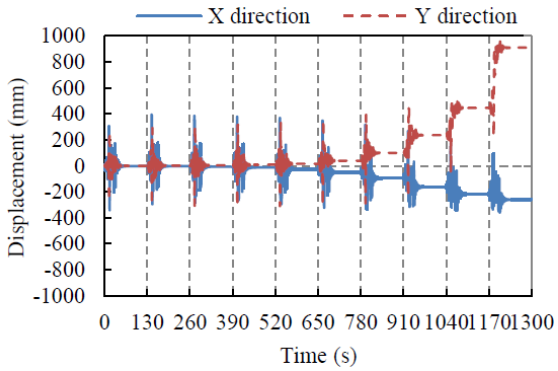


Fig. 19 Displacements of pier top under the swarm type seismic sequence 1244

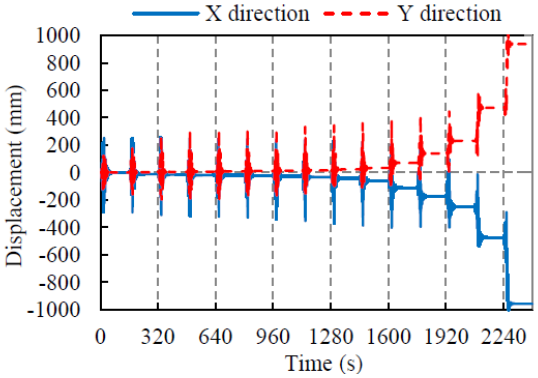


Fig. 20 Displacements of pier top under the swarm type seismic sequence 2752

sum of residual deformation of the pier does not.

Fig. 16, Fig. 17 and Fig. 18 show that there is deviation between the cumulative residual deformation and the sum of residual deformation. It is caused by cumulative damage of the pier under mainshock-aftershock sequences. Moreover, the cumulative residual deformation of the pier increases with the earthquake number under mainshock-aftershock sequences. This indicates that the cumulative effect of residual deformation caused by aftershocks cannot be ignored.

### *5.2 Cumulative residual deformation under swarm type seismic sequences*

The displacements of pier top in X direction and Y direction under swarm type seismic sequences are depicted in Fig. 19 and Fig. 20. It can be seen that the direction of maximum displacement of pier top is offset to the direction of residual deformation, which is caused by the damage in the last earthquake sequence. The residual deformation of the pier increases with the earthquake number, and the increasing rate of residual deformation also increases with the earthquake number. Then damage of pier caused by swarm type seismic sequence is obvious. The pier may be destroyed.

To study the cumulative effect of residual deformation under swarm type seismic sequences, the cumulative residual deformation of the pier are obtained, as shown in Fig. 21 and Fig. 22. In the initial stage of swarm type

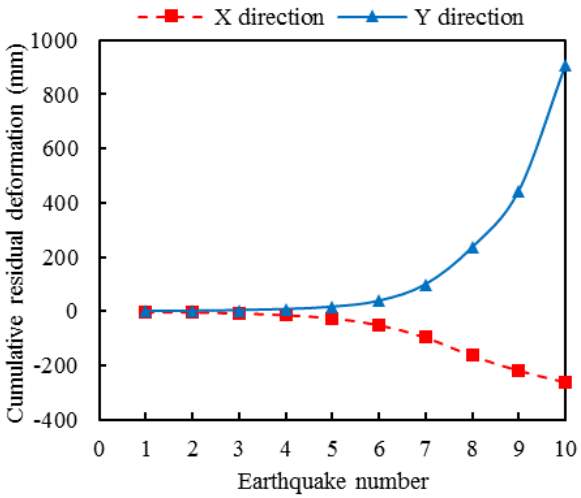


Fig. 21 Cumulative residual deformations of pier under the swarm type seismic sequence 1244

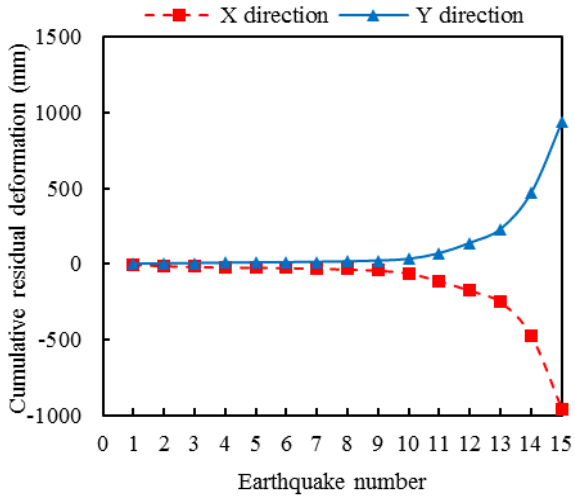


Fig. 22 Cumulative residual deformations of pier under the swarm type seismic sequence 2752

seismic sequences, the cumulative residual deformation of the pier is less than 30 mm. But the cumulative residual deformation of the pier nonlinearly increases with the earthquake number. The reasons are that damage of the pier is accumulated with the increase of earthquake number and the residual deformation of the pier is amplified by the axial pressure of pier top with considering *P-Δ* effect. It shows that .the damage of the pier caused by swarm type seismic sequences is obvious.

## 6. Conclusions

Based on the above investigation, several conclusions can be drawn as follows:

- The cumulative residual deformation of high-speed railway bridge pier under mainshock-aftershock sequences increases with the earthquake number, and the increasing rates are different under different earthquake number. The cumulative effect of residual deformation caused by aftershocks cannot be ignored.
- The cumulative residual deformation of high-speed railway bridge pier under swarm type seismic sequences is nonlinearly related to the earthquake number. Increasing the earthquake number increases the cumulative residual deformation of pier and the increasing rate of cumulative residual deformation.
- The residual deformation of high-speed railway bridge pier under multiple earthquakes is accumulated and even exceeds the limit of code. The cumulative effect of residual deformation cannot be ignored.

## Acknowledgments

The research was funded by the National Natural Science Foundation of China (Grant No. 51878563), the Sichuan Science and Technology Program (Grant No. 2018JY0294 and 2018JY0549), and the Ministry of Science and Technology of China (Grant No. KY201801005).

## Reference

Abbiati, G., Bursi, O.S., Caperan, P., Sarno, L.D., Molina, F.J., Paolacci, F. and Pegon, P. (2015), "Hybrid simulation of a multi-span RC viaduct with plain bars and sliding bearings", *Earthq. Eng. Struct. D.*, **44**(13), 2221-2240. https://doi.org/10.1002/eqe.2580.

Abdelnaby, A.E. and Elnashai, A.S. (2015), "Numerical modeling and analysis of RC frames subjected to multiple earthquakes", *Earthq. Struct.*, **9**(5), 957-981. http://dx.doi.org/10.12989/eas.2015.9.5.957.

Akpınar, U. and Binici, B. (2013), "The effect of infill wall collapse on the deformation estimations of reinforced, concrete frames", *J. Civil Eng. Sci.*, **2**(3), 171-177.

Alessandri, S., Giannini, R. and Paolacci, F. (2013), "Aftershock risk assessment and the decision to open traffic on bridges", *Earthq. Eng. Struct. D.*, **42**, 2255-2275. https://doi.org/10.1002/eqe.2324.

Benavent-Climent, A., Ramirez-Marquez, A. and Pujol, S. (2018), "Seismic strengthening of low-rise reinforced concrete frame structures with masonry infill walls: Shaking-table test", *Eng. Struct.*, **165**, 142-151. https://doi.org/10.1016/j.engstruct.2018.03.026.

Chen, X., Yan, S. and Ji, B.J. (2011), "Pseudo-dynamic test and numerical simulation of high-strength concrete frame structure reinforced with high-strength rebars", *Earthq. Eng. Eng. Vib.*, **10**(2), 303-311. https://doi.org/10.1007/s11803-011-0067-z.

Choi, H., Saiidi, M.S., Somerville, P. and El-Azazy, S. (2010), "Experimental study of reinforced concrete bridge columns subjected to near-fault ground motions", *ACI Struct. J.*, **107**(1), 3-12.

Dai, K.S., Wang, J.Z., Li, B.W. and Hong, H.P. (2017), "Use of residual drift for post-earthquake damage assessment of RC buildings", *Eng. Struct.*, **147**, 242-255. https://doi.org/10.1016/j.engstruct.2017.06.001.

GB 50011-2010 (2010), Code for Seismic Design of Buildings, Ministry of Construction of the People's Republic of China, Beijing, China.

Gou, H.Y., He, Y.N., Zhou, W., Bao, Y. and Chen, G.D. (2018a), "Experimental and numerical investigations of the dynamic responses of an asymmetrical arch railway bridge", *P. I. Mech. Eng. F-J. RAI.*, **232**(9), 2309-2323. https://doi.org/10.1177/0954409718766929.

Gou, H.Y., Long, H., Bao, Y., Chen, G.D., Pu, Q.H. and Kang, R.

(2018b), "Stress distributions in girder-arch-pier connections of long-span continuous rigid frame arch railway bridge", *J. Bridge Eng.*, **23**(7), 04018039. https://doi.org/10.1061/(ASCE)BE.1943-5592.0001250.

Gou, H.Y., Shi, X.Y., Zhou, W., Cui, K. and Pu, Q.H. (2018c), "Dynamic performance of continuous railway bridges: numerical analyses and field tests", *P. I. Mech. Eng. F-J. RAI.*, **232**(3), 936-955. https://doi.org/10.1177/0954409717702019.

Gou, H.Y., Wang, W., Shi, X.Y., Pu, Q.H. and Kang, R. (2018d), "Behavior of steel-concrete composite cable anchorage system", *Steel Compos. Struct.*, **26**(1), 115-123. https://doi.org/10.12989/scs.2018.26.1.115.

Gou, H.Y., Yang, L.C., Leng, D., Bao, Y. and Pu, Q.H. (2018), "Effect of bridge lateral deformation on track geometry of high-speed railway", *Steel Compos. Struct.*, **29**(2), 219-229. https://doi.org/10.12989/scs.2018.29.2.219.

Gou, H.Y., Zhou, W., Chen, G.D., Bao, Y. and Pu, Q.H. (2018e), "In-situ test and dynamic analysis of a double-deck tied-arch bridge", *Steel Compos. Struct.*, **27**(1), 161-175. https://doi.org/10.12989/scs.2018.27.2.161.

Guo, Z.M., Zhang, Y.T., Lu, J.Z. and Fan, J. (2016), "Stiffness degradation-based damage model for RC members and structures using fiber-beam elements", *Earthq. Eng. Eng. Vib.*, **15**(4), 697-714. https://doi.org/10.1007/s11803-016-0359-4.

Han, Z.F., Ye, A.J. and Fan, L.C. (2010), "Effects of riverbed scour on seismic performance of high-rise pile cap foundation", *Earthq. Eng. Eng. Vib.*, **9**(4), 533-543. https://doi.org/10.1007/s11803-010-0035-z.

Hatzigeorgiou, G.D. and Beskos, D.E. (2009), "Inelastic displacement ratios for SDOF structures subjected to repeated earthquakes", *Eng. Struct.*, **31**(11), 2744-2755. https://doi.org/10.1016/j.engstruct.2009.07.002.

Hatzigeorgiou, G.D., Papagiannopoulos, G.A. and Beskos, D.E. (2011), "Evaluation of maximum seismic displacements of SDOF systems from their residual deformation", *Eng. Struct.*, **33**(12), 3422-3431. https://doi.org/10.1016/j.engstruct.2011.07.006.

Jalayer, F. and Ebrahimian, H. (2017), "Seismic risk assessment considering cumulative damage due to aftershocks", *Earthq. Eng. Struct. D.*, **46**, 369-389. https://doi.org/10.1002/eqe.2792.

Jiang, S.Y., Du, C.B. and Hong, Y.W. (2013), "Failure analysis of a cracked concrete gravity dam under earthquake", *Eng. Fail. Anal.*, **33**, 265-280. https://doi.org/10.1016/j.engfailanal.2013.05.024.

Ju, S.H., Leong, C.C. and Ho, Y.S. (2014), "Safety of maglev trains moving on bridges subject to foundation settlements and earthquakes", *J. Bridge Eng.*, **19**(1), 91-100. https://doi.org/10.1061/(ASCE)BE.1943-5592.0000506.

Kostinakis, K. and Morfidis, K. (2017), "The impact of successive earthquakes on the seismic damage of multistorey 3D R/C buildings", *Earthq. Struct.*, **12**(1), 1-12. https://doi.org/10.12989/eas.2017.12.1.001.

Kurt, E.G., Binici, B., Kurç, O., Canbay, E., Akpinar and Ozcebe, G. (2011), "Seismic performance of a deficient reinforced concrete test frame with infill walls", *Earthq. Spectra*, **27**(3), 817-834. https://doi.org/10.1193/1.3609876.

Lee, W.K. and Billington, S.L. (2010), "Modeling residual displacements of concrete bridge columns under earthquake loads using fiber elements", *J. Bridge Eng.*, **15**(3), 240-249. https://doi.org/10.1061/(ASCE)BE.1943-5592.0000059.

Moghaddasi, N.S. and Zhang, Y.F. (2013), "Seismic analysis of diagrid structural frames with shear-link fuse devices", *Earthq. Eng. Eng. Vib.*, **12**(3), 463-472. https://doi.org/10.1007/s11803-013-0186-9.

Omranian, E., Abdelnaby, A.E. and Abdollahzadeh, G. (2018), "Seismic vulnerability assessment of RC skew bridges subjected to mainshock-aftershock sequences", *Soil. Dyn Earthq Eng.*, **114**, 186-197. https://doi.org/10.1016/j.soildyn.2018.07.007.

Pragalath, D.C.H., Bhosale, A., Davis, P.R. and Sarkar, P. (2016), "Multiplication factor for open ground storey buildings-a reliability based evaluation", *Earthq. Eng. Eng. Vib.*, **15**(2), 283-295. https://doi.org/10.1007/s11803-016-0322-4.

Rostamian, M., Hosseinpour, F. and Abdelnaby, A.E. (2017), "Effect of seismic retrofitting on the behavior of RC bridge columns subjected to main shock-aftershock sequences", *Structures Congress*, Denver, CO, June. https://doi.org/10.1061/9780784480403.038.

Ruiz-Garcia, J. and Miranda, E. (2010), "Probabilistic estimation of residual drift demands for seismic assessment of multi-story framed buildings", *Eng. Struct.*, **32**(1), 11-20. https://doi.org/10.1016/j.engstruct.2009.08.010.

Saiidi, M.S. and Ardakani, S.M.S. (2012), "An analytical study of residual displacements in RC bridge columns subjected to near-fault earthquakes", *Bridge Struct.*, **8**(1), 35-45. https://doi.org/10.3233/BRS-2012-0036.

Sakai, J., Jeong, H. and Mahin, S.A. (2005), "Earthquake simulator tests on the mitigation of residual displacements of reinforced concrete bridge columns", *Proceedings of the 21st U.S. -. Japan Bridge Engineering Workshop*, Tsukuba, Japan.

Shafaei, J., Zareian, M.S., Hosseini, A. and Marefat, M.S. (2014), "Effects of joint flexibility on lateral response of reinforced concrete frames", *Eng. Struct.*, **81**(15), 412-431. https://doi.org/10.1016/j.engstruct.2014.09.046.

Sun, Z.Y., Wu, G., Wu, Z.S. and Zhang, J. (2014), "Nonlinear behavior and simulation of concrete columns reinforced by steel-FRP composite bars", *J. Bridge Eng.*, **19**(2), 220-234. https://doi.org/10.1007/s11803-016-0303-7.

Sun, L.M., Xie, W.P., He, X.W. and Hayashikawa, T. (2016), "Prediction and mitigation analysis of ground vibration caused by runing high-speed trains on rigid-frame Viaducts", *Earthq. Eng. Eng. Vib.*, **15**(1), 31-47. https://doi.org/10.1061/(ASCE)BE.1943-5592.0000515.

Sun, Z.Y., Wu, G., Wu, Z.S. and Zhang, J. (2014), "Nonlinear behavior and simulation of concrete columns reinforced by steel-FRP composite bars", *J. Bridge Eng.*, **19**(2), 220-234. https://doi.org/10.1061/(ASCE)BE.1943-5592.0000515.

Tutumluer, E., Qian, Y., Hashash, Y., Ghaboussi, J. and Davis, D.D. (2013), "Discrete element modelling of ballasted track deformation behavior", *Int. J. Rail Trans.*, **1**, 57-73. https://doi.org/10.1080/23248378.2013.788361.

Wu, K.T., Jiao, Y.B., Lv, P.L. and Wang, Z.D (1990), *Introduction to Seismic Sequences*, Peking University Press, March.

Yan, B., Dai, G.L. and Hu, N. (2015), "Recent development of design and construction of short span high-speed railway bridges in China", *Eng. Struct.*, **100**(1), 707-717. https://doi.org/10.1016/j.engstruct.2015.06.050.

Yazgan, U. and Dazio, A. (2011), "Simulating maximum and residual displacements of RC structures: I. Accuracy", *Earthq. Spectra*, **27**(4), 1187-1202. https://doi.org/10.1193/1.3650479.

Yazgan, U. and Dazio, A. (2012), "Post-earthquake damage assessment using residual displacements", *Earthq. Eng. Struct. D.*, **41**(8), 1257-1276. https://doi.org/10.1002/eqe.1184.

Zhang, Q., Zhu, J.C. and Gong, J.X. (2013), "Post-earthquake Residual Deformation Prediction of SDOF System", *J. Civil Arch. Environ. Eng.*, **35**(3), 32-41.

Zhao, J.G., Du, B. and Zhan, Y.L. (2017), "Applicability of mander model in OpenSees for simulation of hysteretic behavior of reinforced concrete column", *J. Lanzhou Univ. Technol.*, **43**(5), 127-133.

Zheng, K.F., Shao, H.T. and Hao, J.J. (2014), "The significance and measures for the globalization of China's high speed railway-overview of the speeches of the guest speakers at the summit on the globalization strategy of China's high speed

railway", *J. Southwest Jiaotong Univ. (Soc. Sci.)*, **15**(1), 1-7.
Zheng, Y.W., Sander, A.C., Rong, W.Y., Fox, P.J., Shing, P.B. and McCartney, J.S. (2018), "Shaking table test of a half-scale geosynthetic-reinforced soil bridge abutment", *Geotech. Test. J.*, **41**(1), 20160268. https://doi.org/10.1520/GTJ20160268.
Zhou, H.L., Fang, G.R., Zhang, A.D., Li, Y.F., Ke, L.S. and Du, Y.H. (1980), "Discussion on judging method of earthquake type", *Earthq. Eng. Eng. Vib*., **2**(2), 47-61.

*CC*